Research Article Vol. 7, No. 10 / October 2020 / Optica 1377

optica

Light trapping in solar cells: simple design rules to maximize absorption

Kezheng Li,[1,†] Sirazul Haque,[2,†] Augusto Martins,[3] Elvira Fortunato,[2] Rodrigo Martins,[2] Manuel J. Mendes,[2] and Christian S. Schuster[1,*]

[1]Department of Physics, University of York, Heslington, York, YO10 5DD, UK
[2]CENIMAT-i3N, Faculdade de Ciências e Tecnologia, Universidade NOVA de Lisboa and CEMOP/UNINOVA, Campus de Caparica, 2829-516 Caparica, Portugal
[3]São Carlos School of Engineering, Department of Electrical and Computer Engineering, University of São Paulo 13566-590, Brazil
*Corresponding author: christian.schuster@york.ac.uk

Received 10 April 2020; revised 22 July 2020; accepted 10 August 2020 (Doc. ID 394885); published 8 October 2020

Solar cells can strongly benefit from optical strategies capable of providing the desired broadband absorption of sunlight and consequent high conversion efficiency. While many diffractive light-trapping structures prove high absorption enhancements, their industrial application rather depends on simplicity concerning the integration to the solar cell concept and the process technology. Here, we show how simple grating lines can perform as well as advanced light-trapping designs. We use a shallow and periodic grating as the basic element of a quasi-random structure, which is highly suitable for industrial mass production. Its checkerboard arrangement breaks the mirror symmetry and is shown, for instance, to enhance the bulk current of a 1 μm slab of crystalline silicon by 125%. We explain its excellent performance by drawing a direct link between a structure's Fourier series and the implied photocurrent, derived from a large and diverse set of structures. Our design rule thus meets all relevant aspects of light-trapping for solar cells, clearing the way for simple, practical, and yet outstanding diffractive structures, with a potential impact beyond photonic applications.

https://doi.org/10.1364/OPTICA.394885

1. INTRODUCTION

Broadband absorption of sunlight is key for solar cell technologies, so nanophotonic structures have emerged as a promising technique for their efficiency improvement. For instance, surface textures enable a reduction in surface reflection, enhancement of internal reflections, and of optical path lengths in the active material [1].

One-dimensional (1D) surface gratings have become one of the most studied diffractive structures. Simple grating lines now serve as test vehicles for theoretical concepts and fabrication methods [2,3]. For example, while their superposition facilitates the analysis of more complicated designs [2,4], gratings are commonly used in monochromators, spectrometers, wavelength-division multiplexing, cavity lasers, and sensors [5]. Some studies also proved their suitability for broadband mirrors [6] and radiative cooling applications [7].

Up to now, simple grating lines have only shown marginal absorption improvements in solar cell materials. The belief that they cannot be the pillar of advanced photonic concepts triggered a new research field to analyze more and more complicated and evermore efficient light-trapping schemes [8–10] at the expense of their complexity. Yet, industry chooses (random) surface textures on the basis of their easy processing and integration in photovoltaic devices. Simple grating lines thus could take a leverage position in large-scale implementations if they outperform state-of-the-art approaches.

However, authors so far typically have focused on specific natural textures or computational algorithms [11]. Even though biological systems show a stunning diversity of surface structures [12–15], they serve multiple functions and result from complex morphological and chemical changes driven by natural selection. To replicate a natural absorption enhancement scheme, we thus first need to translate nature's idea back into simplified terms that are compatible with current fabrication and processing methods. For example, the excellent antireflective properties of foliage surfaces [16,17], insect wings [18], and the moth-eye [19,20] originate from densely packed, gradual-shaped structural features at the subwavelength scale. Similarly, we can mimic these structures with artificially nanostructured arrays of domes, pillars, cones, or pyramids on solar cells [21–23].

The focus has recently moved from the actual texture to its scattering and diffraction pattern. In fact, the absorption enhancement by rose petals [24,25] and tropical butterfly wings [26–28] originates from refractive and diffractive effects, respectively. Some studies try to link the superiority of a structure to the lower symmetry in its diffraction pattern [29,30], but others refrain from conclusions based on symmetry group theory alone [31].

Corrected 20 November 2020

For example, the comparison of the dimple and rose structure in Ref. [29] shows that coupling to higher diffraction orders does not necessarily translate to a greater current enhancement than coupling to lower orders. The actual principle for efficient light-trapping thus remains unclear.

If structural features cannot explain why some structures perform better than others, the research question must be approached from a different perspective. Here, we outline how a basic principle empowers grating lines to outperform state-of-the-art literature proposals. Finally, from a survey of a large and diverse range of structures, we derive four design criteria that directly link the Fourier series of a structure to its implied photocurrent. They enable us, in turn, to explain the excellent performance of our design principle. It thus generally applies and is not restricted to particular structural features or the material.

2. THEORETICAL CONSIDERATIONS

A. Grating Lines

Simple grating lines are often regarded as disadvantageous, because one-dimensionality cannot address both polarization states effectively at the same time. Lines mostly affect the absorption enhancement of a plane of incident angles instead of the full hemisphere. In addition, high periodicity leads to sharp and not broad resonance peaks in the absorption spectrum, restricting the absorption enhancement to only narrow wavelength intervals.

Once we look at two-dimensionality, such as crossed 1D grating lines, we note a substantial gain in photocurrent compared to their 1D counterpart. Could two-dimensional (2D) periodicity cause this effect? In fact, 2D periodic textures have received much interest due to their potential for higher light-trapping improvement over random textures [4,23,32]. Gjessing *et al.* optimized seven different 2D periodic structures [29]. Although they found the lattice period that gives optimal light trapping is comparable for all structures, the light-trapping ability differs between them. 2D periodicity thus cannot solely explain the high performance of a light-trapping structure.

However, when an appropriate level of short-range disorder is tuned into the structure via its Fourier-space representation, a better light-trapping solution is found [2,33,34]. Accordingly, the search for the optimum optical scheme has led to apparently randomly distributed geometrical features arranged inside a large, periodically repeated unit cell.

In principle, the light-trapping problem then appears as solved by quasi-random (QR) nanostructures. However, a diffraction pattern does not define the desired structure. The abstract concept of Fourier-space engineering may not give clear guidance to a technologist, particularly in terms of simple fabrication and processing techniques. The opposite is instead a more natural approach, i.e., arranging simple periodic structures in a QR manner.

This proposal might be the way out for grating lines to overcome the one-dimensionality issue and to gain a quasi-randomness appearance at the same time. In fact, we can show that the two approaches are complementary solutions to the light-trapping problem. Yet, gratings show distinct advantages for solar cell applications, as we highlight in the discussion section.

Fig. 1. Depiction of different arrangements of diffractive elements (photonic domains) in square lattice structures. The rose (left) and zigzag (center) structure are based on the same diffractive element, i.e., a monopitched roof [29], which is rotated 90 deg four times. The checkerboard structure (right) results from the simplification of the monopitched roof as a nonslanted grating line. Since all photonic domains contain one element, the computational unit cell encloses four.

B. Photonic Domain

Commonly, a unit cell defines the region of interest for optical (electromagnetic) modeling. It encloses the surface structure in a square or rectangle, to which periodic boundary conditions are applied to ease the simulation. While a convenient technique for computational analysis, this method does not highlight the relationship between the geometrical arrangement of the diffractive features and their unit cell.

To simplify the following discussion, we introduce the concept of the photonic domain. We define it as the region within a photonic structure in which a basic diffractive element is periodically arranged in a 1D fashion. But the domain could comprise just a single element, too. For example, Gjessing *et al.* [29] used a monopitched roof as the building block, i.e., the photonic domain, for the rose and zigzag structures shown in Fig. 1. Before displacing a roof next to another one, it is rotated by 90 deg.

Therefore, it may not be difficult to increase the apparent randomness of a design with periodic grating lines. When we replace the monopitched roof of the rose or zigzag structure with lines, we get the checkerboard pattern shown in Fig. 2(c). Such trellised patterns were proposed to control the wetting properties of surfaces [35], but have so far not been analyzed for light-trapping applications.

In addition, changing the shape of the photonic domain increases the design freedom. Whereas triangular, rectangular, and hexagonal domains have been studied in the field [30,36,37], only a few authors proposed a pentagonal or heptagonal domain for light-trapping despite their superior characteristics [38]. But as the regular pentagon has a 72 deg rotational symmetry, it cannot tile a plane alone [39]. In Fig. 2(d), we thus propose an irregular pentagon with two different side lengths as the photonic domain for efficient light trapping. Curiously, the alternate arrangement of such pentagons enables butterfly wings to absorb more sunlight [15,19,26,27].

Finally, modulating grating lines with a rotational operator, as in the farrago design [Fig. 2(e)], allows one to quantify the introduced level of "randomness" by the number of differing domains, e.g., two for the zigzag, checkerboard, or pentagon, four for the rose, and 72 for the farrago.

3. RESULTS

We first optimize the checkerboard structure shown in Fig. 2(c). As its photonic domain comprises a 1D grating only, the structure becomes defined solely by three design parameters: the side length

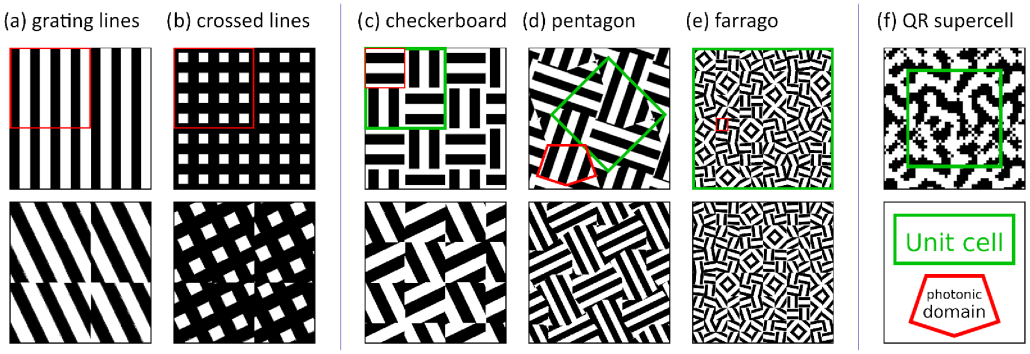

Fig. 2. (a)–(e) Arrangement of a simple diffractive element controls the structural disorder. While periodicity can be disturbed via restructured photonic domains (bottom), this approach does not break mirror symmetry. Superior light-trapping structures repeat a (e) periodic element quasi-randomly or a (f) QR element periodically. Whereas the former case offers flexibility in its design, fabrication, and modification, the latter relies on accurate replication techniques. Since the unit cell is also the photonic domain of the QR supercell, design (f) from Ref. [33] cannot be generated from the QR arrangement of a periodic element—in contrast to designs (c)–(e).

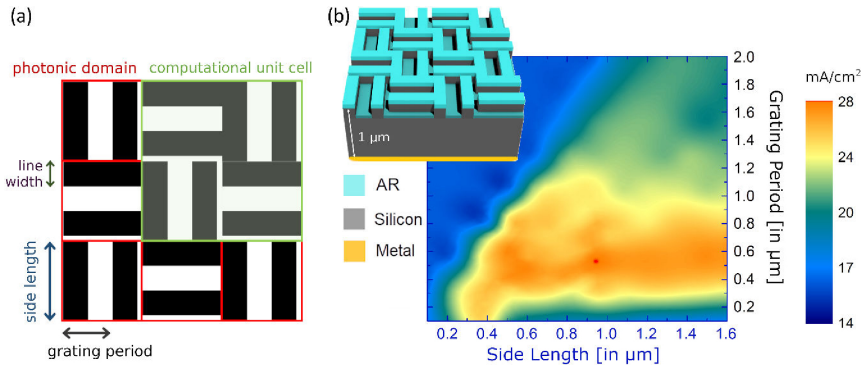

Fig. 3. (a) Representation of the checkerboard's photonic domain and computational unit cell. (b) The parameter map shows the computed maximum achievable photocurrent density J_{max} as a function of the grating period and domain size. The inset shows the test cell with the checkerboard structure over it. The linewidth is here kept at half the grating period. The red dot marks the optimal parameter set that maximizes the broadband absorption in the 1 µm c-Si layer.

of the photonic domain, the grating's line width, and its period; see Fig. 3(a).

For a direct comparison of light-trapping performance, we follow the strategy set out in previous works [33,37,40,41], employing a test solar cell structure composed of a crystalline silicon (c-Si) absorber material [42] with an ideal back reflector:

- The thickness of the c-Si slab is set to 1 µm. At this thickness, light trapping has a great impact on absorption, and differences in photocurrent will manifest noticeably in the comparison of different textures [37].
- All photonic domains are etched on the front surface, whose depth is fixed at 190 nm, which was found optimal in previous studies [33,40] for a 1 µm thickness.
- The c-Si surface is coated with a transparent dielectric medium of refractive index 1.65 and 70 nm thickness, conformally. This layer acts both as a passivating film for the etched regions as well as an antireflection coating.

The photocurrent density produced in the c-Si material is taken as the figure of merit. It is equivalent to the maximum achievable photocurrent density J_{max} that would be generated by the cell. Here, we use the software package Lumerical FDTD Solutions to calculate J_{max} (see Supplement 1 for a brief description of the simulation) over the main spectral range of the AM1.5 G solar spectrum, i.e., from 315 to 1150 nm wavelength.

From the parameter scan depicted in Fig. 3(b), we identify a high photocurrent region for grating periods between 0.3 and 0.9 µm, with the optimum period and domain size around 575 nm and 0.925 × 0.925 µm^2, respectively. Next, as the linewidth was kept at half of the grating period, we now study the impact of the linewidth on the J_{max}. We find 242 nm as the best parameter (see Fig. S1 in Supplement 1); that matches the linewidth of the optimized crossed grating design. Surprisingly, the checkerboard arrangement (28.4 mA/cm^2) considerably outperforms the crossed design (25.2 mA/cm^2), as shown in Fig. 4, and demonstrates an excellent angular insensitivity up to a 60-degree angle of incidence, as shown in Fig. S2 (see Supplement 1). The structure surpasses recent proposals [40,43–45] and even rivals the exceptional performance of the QR supercell [33]; see Tables 1 and 2 and Figs. S3–S5 in Supplement 1. This sophisticated design is termed supercell, because the superposition of multiple gratings (with the same period) controls the phase shift between its diffraction orders [2].

To verify that our parameter optimization was indeed unconditional, we extended our finite-difference time domain (FDTD) calculations to different domain sizes, as reported in Fig. S6 of

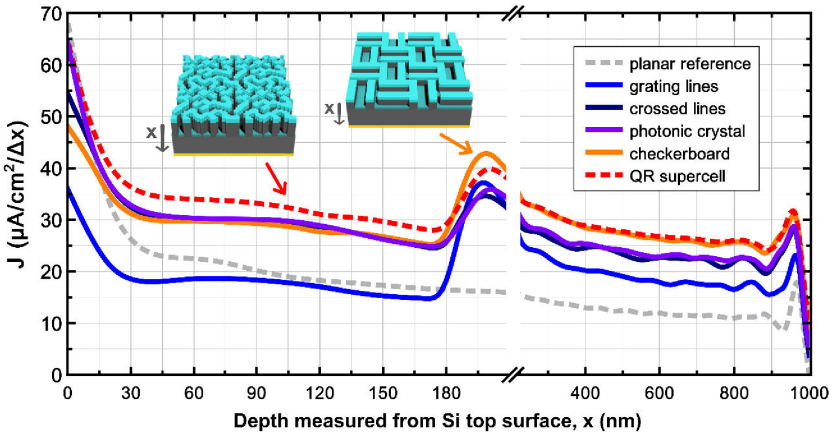

Fig. 4. Photocurrent depth profile, i.e., current generation per unit volume as a function of the absorber's depth x, determined by segmenting the total (1 μm) c-Si slab in thin slices with a step size of $\Delta x = 10$ nm. All current density profiles are calculated for the AM1.5 G solar spectrum. While the current J generated in the surface pattern (0–190 nm depth) is equal for the checkerboard, photonic crystal, and crossed grating lines, the current in the flat bulk layer (190–1000 nm depth) is the same for the checkerboard and supercell design from Ref. [33]. Although the highest current is found within the QR supercell's surface texture, it will likely suffer the most from surface recombination effects (see Fig. S8 in Supplement 1).

Table 1. Recent Theoretical Proposals for Light-Trapping in Thin-Film c-Si Solar Cells[a]

Structure Name	Total c-Si Slab Thickness (μm)	LTE	Maximum Current (mA/cm²)
Grating lines [this study]	1.0	0.31	19.5
Retina's fovea [43]	3.1	0.65	21.6
1D periodic Fourier-series profile [44]	1.3	0.66	24.6
Crossed lines [this study]	1.0	0.68	25.2
Photonic crystal [40]	1.0	0.73	25.9
Begonia's spiral [45]	1.5	0.83	26.2
Leaf-inspired scheme [46]	20.0	0.87	28.0
Checkerboard [this study]	1.0	0.89	28.4
QR supercell [33]	1.0	0.96	29.5

[a]The crossed grating lines have a 242 nm width. The light-trapping efficiency (LTE) compares the actual current gain via surface structuring to the theoretical current gain via Lambertian scattering [8]. It thus aims at assessing the performance of the nanostructure itself, irrespective of the fabrication method and technology used. J_{max} not found in a reference were calculated using the published absorption spectra.

Supplement 1. Furthermore, we also changed the domain geometry from a square to an irregular pentagon with two different side lengths, as shown in Fig. 2(d), effectively adding a degree of freedom to the design. Yet, we optimized the pentagon only tentatively due to computational restraints (see Fig. S7 in Supplement 1) because we preferred to focus on the checkerboard's simpler geometry. Additional optimization steps thus may well reveal the pentagon's benefit.

Four parameters thus define our proposed light-trapping solution: the photonic domain size, the structural feature size, their periodicity, and the etching depth. Table 2 summarizes the transformative steps undergone by the photonic domain and the resulting quantitative changes in the J_{max}, which we cross-checked with a different simulation method (rigorous coupled wave analysis).

4. DISCUSSION

A. Real-Space Considerations

Just as hierarchical structures in biological systems often vary a certain building block [14], we generate a set of different domains via the modulation of a basic photonic element. As such, a set defines a unit cell dynamically; our simple principle introduces a new class of light-trapping structures, like the checkerboard, farrago, or pentagon patterns shown in Fig. 2.

Here, we focus on the checkerboard pattern that results from the displacement and $\pi/2$ rotation of periodic grating lines. This alternate arrangement increases the bulk current by twice as much

Table 2. Potential Impact of Surface Structures on the Carrier Generation under AM1.5 G Solar Spectrum[a]

Photonic Structure	Domain Length (μm)	Unit Cell			Surface Current (mA/cm²)	Bulk Current (mA/cm²)
		Size (μm²)	FF (%)	Surface Area Increase (%)		
Planar reference	NA	NA	0	0	4.6	10.1
Grating lines	0.575	0.33	58	66	3.6	16.0
Crossed lines	0.575	0.33	34	77	5.9	19.3
Checkerboard	0.925	3.42	48	82	5.8	22.7
Photonic crystal [40]	0.600	0.36	35	66	6.1	19.9
QR supercell [33]	1.792	3.21	50	188	6.6	22.9

[a]All grating lines have a 242 nm width. The filling factor FF is defined as the area of the etched regions over the entire area of the unit cell. The surface/bulk current refers to carriers generated within/beyond 190 nm depth. Remarkably, grating lines can enhance the bulk current of a 1 μm thin c-Si slab by 125% via the checkerboard arrangement.

as a crossing of the lines can do. Therefore, the checkerboard light-trapping performance is close to that of the QR supercell design.

However, although both structures use the same silicon volume, the QR supercell has a 60% larger surface area (cf. Table 2) that increases surface recombination effects [47], as evident from its carrier generation profile (see Fig. S8 in Supplement 1). In a preliminary experiment on commercial cells, we could also observe how these effects scale with the surface area to volume ratio. Therefore, we note the checkerboard's ability to shift its carrier generation further into the bulk, accomplished by

- choosing an up to 30% smaller linewidth (shown in Fig. S1 in Supplement 1),
- using an up to 30% shallower etching depth (see Fig. S5 in Supplement 1),
- extending its unit cell to three domains via $\pi/3$-rotated grating lines (see Fig. S9 in Supplement 1).

Consequently, the tolerance in width and depth of the large rectangular features makes the checkerboard structure more robust to fabrication imperfections. Noise in the linewidth may improve its angular response [18,48], and tapered lines couple better to incident light [49] as the optical density changes more gradually. The checkerboard thus mainly depends on the grating period, as shown in Fig. 3(b), permitting a fast turnaround from the design to its implementation up to potential modifications.

Since light beyond 600 nm wavelength is not absorbed within a double pass of the 1 μm silicon slab, one could select $\lambda_0 = 600$ nm as the target wavelength, which in turn would define the grating period $P \approx \lambda_0$. If the grating height h and duty cycle D are then chosen such that the zero diffraction order cancels out, light will be transmitted only at odd diffraction orders. So, the phase difference $\Delta\phi = 2\pi/\lambda_0 * h * \Delta n$ of the interfering waves must be equal to π and $D = 50\%$ [50,51], implicating $h = \lambda_0/(2{\cdot}\Delta n) \approx 130$ nm for an index contrast of $\Delta n = n_{\mathrm{Si}} - n_{\mathrm{ARC}} = 2.29$ at $\lambda_0 = 600$ nm. We note that these preliminary estimates are remarkably close to the outcome of the intensive FDTD computations performed in this work.

In addition, we also analyzed the checkerboard's performance to nonstructural variations in Fig. S10 of Supplement 1 but found only 3% to 4% differences when the coating and c-Si layer thickness vary by 15% and 10%, respectively.

Finally, our study was motivated by the desire to reduce design complexity without loss in light-trapping performances. While the small 32 nm pixels of the QR supercell structure can raise complications in all the here-mentioned lithography approaches, the simplicity of the checkerboard structure does not rely on a sophisticated fabrication technique: grating profiles are widely manufactured by holographic techniques, such as laser interference lithography, but also qualify for high-speed electron (multi) beam lithography [52–54]. Submicrometer gratings can also be imprinted [55]. For example, Hamamatsu uses nanoimprinted gratings for its ultracompact minispectrometers, whereas Canon teamed up with Toshiba to develop 15 nm nanoimprint lithography for the high-volume manufacturing of semiconductor devices [56]. Immersion lithography, deep UV lithography, and digital planar holography are other industrial methods. We would like to note that displacement Talbot lithography (DTL) [57,58] could be a promising large-area lithography technique for the checkerboard structure. However, as the current state of the art seems to focus on strictly periodic patterns, it appears that only a direct writing is capable of generating checkerboard patterns. As such, their feasibility remains to be tested. While some QR [59] and complex periodic structures [60] were already produced via DTL, preliminary simulations seem to indicate that DTL might in principle be able to create the checkerboard structure as well [61].

B. Fourier-Space Considerations

After highlighting the practical advantages of the checkerboard design, we now turn to the question of why its performance rivals the one from the QR supercell approach, whose functionality was tuned into its structure via Fourier-space considerations. In fact, the Fourier spectrum of the QR supercell is rich, thereby giving the appearance of continuity, and concentrates all its energy distribution function $\mathrm{ED}(k_x, k_y)$ in a ring region between 10 $\mu\mathrm{m}^{-1}$ and 25 $\mu\mathrm{m}^{-1}$; see Fig. 5(a). In contrast, the checkerboard's Fourier spectrum is not very broad and is mainly distributed along the principal axis; see Fig. 5(b). Still, both designs yield high performances.

So, could the supercell concept ignore classes of structures that fail its ring criteria? This question inspired us to analyze the Fourier series of a vast range of diverse structures (see Table S1 in Supplement 1), enabling us to identify four criteria that correlate with current gains:

1. high number N_{strong} of strong Fourier series components;
2. low contribution of strong components $\mathrm{ED}_{\mathrm{strong}}$ to the total diffracted energy $\mathrm{ED}_{\mathrm{tot}}$—a component is defined as strong (weak) if its Fourier energy exceeds (falls below) n% of the series' peak value;
3. low energy spread into the outer k region $\mathrm{ED}_{k>k^*}$, i.e., beyond the wavenumber k^*;
4. high surface area factor (SAF) of the pattern—the SAF quantifies the increase in surface area compared to an unstructured slab while respecting the periodic boundary conditions of the unit cell.

It is $\mathrm{ED}_{\mathrm{weak}} + \mathrm{ED}_{\mathrm{strong}} = \mathrm{ED}_{\mathrm{tot}}$ and $\mathrm{ED}_{k<k^*} + \mathrm{ED}_{k>k^*} = \mathrm{ED}_{\mathrm{tot}}$. Our extensive study reveals a direct link between the Fourier properties of a light-trapping structure and its resulting theoretical current enhancement $X = J_{\mathrm{max}}/J_{\mathrm{ref}}$ of a 1 μm c-Si slab, here empirically defined by

$$X = 1 + (1 - \sqrt{f})^p$$

$$\text{with} \quad 1/f = \mathrm{SAF} \cdot \sqrt{\frac{\mathrm{ED}_{\mathrm{weak}}}{\mathrm{ED}_{k>k^*}}} \cdot N_{\mathrm{strong}}^q \cdot \left(\frac{\mathrm{ED}_{k<k^*}}{\mathrm{ED}_{\mathrm{strong}}}\right)^p \qquad (1)$$

in which the function $1/f$ evaluates the four criteria in k space, quantitatively. We find a high correlation coefficient $R = 0.97$ between X and J_{max} for $p = 1.87$ and $q = 1.19$, which is robust to changes in n or k^* and is maximal for $n = 15$ and $k^* = 21$ $\mu\mathrm{m}^{-1}$ (see Table S2 in Supplement 1). According to Fig. 6, the point $X = 1.7$ separates the surface structures with a single domain from those that yield the highest J_{max}.

Since our design principle meets the four criteria better than (crossed) grating lines alone, the checkerboard rivals the QR supercell structure, whose design does still fulfill them best:

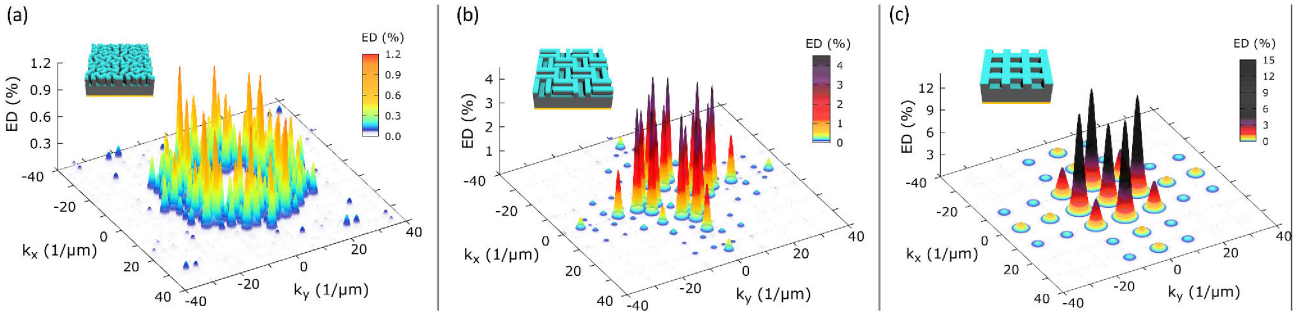

Fig. 5. Fourier energy spectrum in k space for (a) the QR supercell, (b) the checkerboard, and (c) the crossed lines. For comparison, the energy distribution ED(k_x, k_y) is normalized to the total diffracted intensity, given by the sum of all Fourier components in k space. Here, each structure covers a 500 μm^2 area in real space; it is sampled at 5 nm resolution and expressed as a binary data matrix. Its Fourier transformation yields the desired Fourier-series components (after shifting the zero-frequency component to the center of the array). For their visualization only, they were appropriately smoothed.

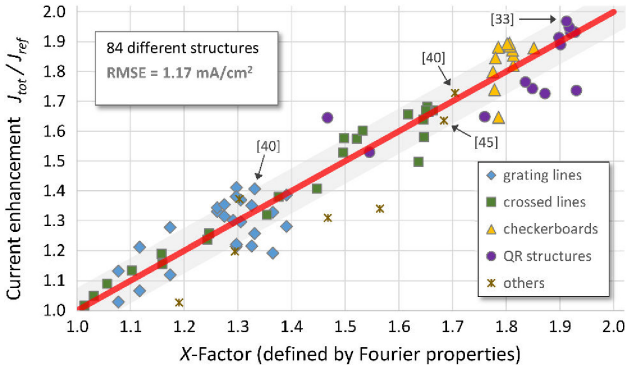

Fig. 6. Analysis of 84 different surface structures that are etched 190 nm into a 1 μm thin c-Si slab (listed in Table S1 Supplement 1), indicates a link between their Fourier properties [Eq. (1)] and the theoretical maximum achievable photocurrent $J_{max} = X \cdot J_{ref}$, with the planar reference $J_{ref} = 15$ mA/cm^2. Some selected literature proposals are annotated with their references in brackets. For a fair comparison, all Fourier series are based on the same aperture area of ca. 500 μm^2, sampled at 5 nm resolution and expressed as a binary data matrix. Although the root mean square error RMSE (gray-toned area) implies a forecast that is often greater than the mean absolute percentage error (4.2%), the correlation coefficient R highlights a strong relationship between X and J_{max}. In fact, the mean absolute scaled error (63%) shows that our (red) trendline is almost twice as good as the naïve model.

(a) uniformity in k space increases the number of strong components N_{strong} but also weakens their contribution (criteria 1 and 2);
(b) limiting the diffraction pattern to $k = 24.5$ μm^{-1}, that is close to $k^* = 21$ μm^{-1} (criterion 3);
(c) the choice of small and squared pixels increases the SAF (criterion 4).

However, suppressing the lowest orders, as in Fig. 5(a), is not necessary (shown in Fig. S11 in Supplement 1): their inclusion reduces the surface current by 0.5 mA/cm^2 but increases the bulk current by 0.2 mA/cm^2 (cf. QR32_E0-E7 in Table S1), resulting in only a 0.3 mA/cm^2 lower photocurrent than the J_{max} of the original QR supercell design (cf. QR32b in Table S1).

Finally, since light-trapping structures inherently boost the surface recombination [47], considering this effect in the analysis relies on a full-device modeling approach and, therefore, greatly complicates the comparison of multiple proposals. We argue that the best light-trapping structure generates the greatest bulk current with the smallest increase in surface area. As such, when using the same surface passivation technology, the checkerboard structure will likely outperform the QR supercell design.

5. CONCLUSIONS

Surface textures increase the absorption of sunlight in photovoltaic materials. Although this strategy led to powerful designs, proposals often neglect their technological practicalities. For example, engineering the desired diffraction pattern into a structure via its k space representation may result in its arbitrary appearance in real space, e.g., the QR supercell approach. Such a fine-tuned structure then becomes difficult to fabricate on a large scale, to monitor for imperfections, and to modify if needed later on.

Here, we move the focus from the structure to the arrangement of its basic element. We outline how arranging grating lines yields the same high performance of sophisticated designs but with practical advantages. We thereby introduce the concept of the photonic domain and show how the combination of Fourier analysis and current depth profile allows one to fully assess all relevant aspects of light-trapping designs for solar cells. For example, the checkerboard pattern shows much simplicity in design, reduced surface area, and high robustness to imperfections.

While we restricted our work to the cell level, any encapsulation material and protective glass cover will unlikely affect our conclusions. We expect their presence to reduce the charge generation in the surface structures. In addition, our concepts were tested on a 1 μm slab of c-Si. Therefore, changing the etching depth, absorber thickness, or its material inevitably changes the optimal design parameters in real and Fourier space; both will be subject to a follow-up study. Whereas the supercell lacks a suitable parameter set to track such modifications, because its design must always be visualized and cannot be read off a current map, the checkerboard's optimal parameters can be listed in a look-up table or even intuitively found experimentally.

We expect our simple design principle to impact not only in the solar cell or LED sector but also in applications where a disruptive function is required on large areas, such as acoustic noise shields, wind break panels, anti-skid surfaces, liquid control devices [35], biosensors, and atomic cooling [62].

Funding. Fundação para a Ciência e a Tecnologia (PD/BD/143031/2018, PTDC/EAM-PEC/29905/2017, PTDC/NAN-OPT/28430/2017, PTDC/NAN-OPT/28837/2017,

UID/CTM/50025/2019); Fundação de Amparo à Pesquisa do Estado de São Paulo (2015/21455-1); Engineering and Physical Sciences Research Council (EP/P02324X/1).

Acknowledgment. K. Li acknowledges support by the EPSRC. A. Martins is grateful for support by the São Paulo Research Foundation (FAPESP). S. Haque acknowledges support from FCT/MCTES through the AdvaMTech PhD program scholarship PD/BD/143031/2018. C. Schuster thanks the University of York for associate membership, the Institute of Physics for the Carers' Fund and the Benevolent Fund, and S. Castillo Avila for encouragement and continuous support, particularly over the past three years.

Disclosures. The authors declare no conflicts of interest.

See Supplement 1 for supporting content.

[†]These authors contributed equally to this work.

REFERENCES

1. M. L. Brongersma, Y. Cui, and S. Fan, "Light management for photovoltaics using high-index nanostructures," Nat. Mater. **13**, 451–460 (2014).
2. E. R. Martins, J. Li, Y. Liu, J. Zhou, and T. F. Krauss, "Engineering gratings for light trapping in photovoltaics: the supercell concept," Phys. Rev. B **86**, 041404 (2012).
3. S. Schauer, R. Schmager, R. Hünig, K. Ding, U. W. Paetzold, U. Lemmer, M. Worgull, H. Hölscher, and G. Gomard, "Disordered diffraction gratings tailored by shape-memory based wrinkling and their application to photovoltaics," Opt. Mater. Express **8**, 184–198 (2018).
4. R. Dewan, S. Shrestha, V. Jovanov, J. Hüpkes, K. Bittkau, and D. Knipp, "Random versus periodic: determining light trapping of randomly textured thin film solar cells by the superposition of periodic surface textures," Sol. Energy Mater. Sol. Cells **143**, 183–189 (2015).
5. P. Kozma, A. Hamori, K. Cottier, S. Kurunczi, and R. Horvath, "Grating coupled interferometry for optical sensing," Appl. Phys. B **97**, 5–8 (2009).
6. C. F. R. Mateus, M. C. Y. Huang, L. Chen, C. J. Chang-Hasnain, and Y. Suzuki, "Broad-band mirror (1.12–1.62μm) using a subwavelength grating," IEEE Photon. Technol. Lett. **16**, 1676–1678 (2004).
7. A. Hervé, J. Drévillon, Y. Ezzahri, and K. Joulain, "Radiative cooling by tailoring surfaces with microstructures: association of a grating and a multi-layer structure," J. Quant. Spectrosc. Radiat. Transf. **221**, 155–163 (2018).
8. C. S. Schuster, A. Bozzola, L. C. Andreani, and T. F. Krauss, "How to assess light trapping structures versus a Lambertian scatterer for solar cells?" Opt. Express **22**, A542–A551 (2014).
9. S. Morawiec, J. Holovský, M. J. Mendes, M. Müller, K. Ganzerová, A. Vetushka, M. Ledinský, F. Priolo, A. Fejfar, and I. Crupi, "Experimental quantification of useful and parasitic absorption of light in plasmon-enhanced thin silicon films for solar cells application," Sci. Rep. **6**, 22481 (2016).
10. A. Araújo, M. J. Mendes, T. Mateus, J. Costa, D. Nunes, E. Fortunato, H. Águas, and R. Martins, "Ultra-fast plasmonic back reflectors production for light trapping in thin Si solar cells," Sol. Energy **174**, 786–792 (2018).
11. R. A. Gouvêa, M. L. Moreira, and J. A. Souza, "Evolutionary design algorithm for optimal light trapping in solar cells," J. Appl. Phys. **125**, 043105 (2019).
12. W. Barthlott, M. Mail, B. Bhushan, and K. Koch, "Plant surfaces: structures and functions for biomimetic innovations," Nano-Micro Lett. **9**, 23 (2017).
13. P. Ball, "Life's lessons in design," Nature **409**, 413–416 (2001).
14. B. Bhushan, "Biomimetics: lessons from nature–an overview," Philos. Trans. R. Soc. A **367**, 1445–1486 (2009).
15. Z. Han, Z. Mu, W. Yin, W. Li, S. Niu, J. Zhang, and L. Ren, "Biomimetic multifunctional surfaces inspired from animals," Adv. Colloid Interface Sci. **234**, 27–50 (2016).
16. Z. Huang, S. Yang, H. Zhang, M. Zhang, and W. Cao, "Replication of leaf surface structures for light harvesting," Sci. Rep. **5**, 14281 (2015).
17. Z. Huang, T. Shi, H. Zhang, M. Zhang, M. Huttula, and W. Cao, "A computational study of antireflection structures bio-mimicked from leaf surface morphologies," Sol. Energy **131**, 131–137 (2016).
18. R. H. Siddique, G. Gomard, and H. Hölscher, "The role of random nanostructures for the omnidirectional anti-reflection properties of the glasswing butterfly," Nat. Commun. **6**, 6909 (2015).
19. Z. W. Han, Z. Wang, X. M. Feng, B. Li, Z. Z. Mu, J. Q. Zhang, S. C. Niu, and L. Q. Ren, "Antireflective surface inspired from biology: a review," Biosurf. Biotribol. **2**, 137–150 (2016).
20. J. Sun, X. Wang, J. Wu, C. Jiang, J. Shen, M. A. Cooper, X. Zheng, Y. Liu, Z. Yang, and D. Wu, "Biomimetic moth-eye nanofabrication: enhanced antireflection with superior self-cleaning characteristic," Sci. Rep. **8**, 5438 (2018).
21. O. Sanchez-Sobrado, M. J. Mendes, S. Haque, T. Mateus, A. Araujo, H. Aguas, E. Fortunato, and R. Martins, "Colloidal-lithographed TiO_2 photonic nanostructures for solar cell light trapping," J. Mater. Chem. C **5**, 6852–6861 (2017).
22. M. J. Mendes, A. Araújo, A. Vicente, H. Águas, I. Ferreira, E. Fortunato, and R. Martins, "Design of optimized wave-optical spheroidal nanostructures for photonic-enhanced solar cells," Nano Energy **26**, 286–296 (2016).
23. S. Haque, M. J. Mendes, O. Sanchez-Sobrado, H. Águas, E. Fortunato, and R. Martins, "Photonic-structured TiO_2 for high-efficiency, flexible and stable perovskite solar cells," Nano Energy **59**, 91–101 (2019).
24. R. Hünig, A. Mertens, M. Stephan, A. Schulz, B. Richter, M. Hetterich, M. Powalla, U. Lemmer, A. Colsmann, and G. Gomard, "Flower power: exploiting plants' epidermal structures for enhanced light harvesting in thin-film solar cells," Adv. Opt. Mater. **4**, 1487–1493 (2016).
25. K. Li, R. Wu, Y. Ruan, L. Zhang, and H. Zhen, "Numerical analysis of the angular insensitive photovoltaic light harvesting with the biomimetic scattering film inspired by the rose petal epidermal topography," Sol. Energy **170**, 800–806 (2018).
26. Z. Han, S. Niu, C. Shang, Z. Liu, and L. Ren, "Light trapping structures in wing scales of butterfly *Trogonoptera brookiana*," Nanoscale **4**, 2879–2883 (2012).
27. Z. Han, Z. Mu, B. Li, S. Niu, J. Zhang, and L. Ren, "A high-transmission, multiple antireflective surface inspired from bilayer 3D ultrafine hierarchical structures in butterfly wing scales," Small **12**, 713–720 (2016).
28. R. H. Siddique, Y. J. Donie, G. Gomard, S. Yalamanchili, T. Merdzhanova, U. Lemmer, and H. Hölscher, "Bioinspired phase-separated disordered nanostructures for thin photovoltaic absorbers," Sci. Adv. **3**, e1700232 (2017).
29. J. Gjessing, A. S. Sudbø, and E. S. Marstein, "Comparison of periodic light-trapping structures in thin crystalline silicon solar cells," J. Appl. Phys. **110**, 033104 (2011).
30. S. E. Han and G. Chen, "Toward the Lambertian limit of light trapping in thin nanostructured silicon solar cells," Nano Lett. **10**, 4692–4696 (2010).
31. T. Cai and S. E. Han, "Effect of symmetry in periodic nanostructures on light trapping in thin film solar cells," J. Opt. Soc. Am. B **32**, 2264–2270 (2015).
32. C. Battaglia, C.-M. Hsu, K. Söderström, J. Escarré, F.-J. Haug, M. Charrière, M. Boccard, M. Despeisse, D. T. L. Alexander, M. Cantoni, Y. Cui, and C. Ballif, "Light trapping in solar cells: can periodic beat random?" ACS Nano **6**, 2790–2797 (2012).
33. E. R. Martins, J. Li, Y. Liu, V. Depauw, Z. Chen, J. Zhou, and T. F. Krauss, "Deterministic quasi-random nanostructures for photon control," Nat. Commun. **4**, 2665 (2013).
34. W.-K. Lee, S. Yu, C. J. Engel, T. Reese, D. Rhee, W. Chen, and T. W. Odom, "Concurrent design of quasi-random photonic nanostructures," Proc. Natl. Acad. Sci. USA **114**, 8734–8739 (2017).
35. X. Zhang, Y. Cai, and Y. Mi, "Anisotropic wetting on checkerboard-patterned surfaces," Langmuir **27**, 9630–9637 (2011).
36. Z. Yu, A. Raman, and S. Fan, "Fundamental limit of nanophotonic light-trapping in solar cells," Proc. Natl. Acad. Sci. USA **107**, 17491–17496 (2010).
37. P. Wang and I. M. Peters, "Impact of structure symmetry on light trapping properties of periodic nanostructures: a systematic discussion and quantification," J. Appl. Phys. **119**, 083101 (2016).

38. X. Guo, D. Wang, B. Liu, Y. Zhou, and S. Li, "Quick design of high efficiency light trapping nanostructures for thin film silicon solar cells," Opt. Commun. **395**, 122–126 (2017).
39. "The Nobel Prize in chemistry 2011," https://www.nobelprize.org/prizes/chemistry/2011/press-release/.
40. A. Bozzola, M. Liscidini, and L. C. Andreani, "Photonic light-trapping versus Lambertian limits in thin film silicon solar cells with 1D and 2D periodic patterns," Opt. Express **20**, A224–A244 (2012).
41. S. Zanotto, M. Liscidini, and L. C. Andreani, "Light trapping regimes in thin-film silicon solar cells with a photonic pattern," Opt. Express **18**, 4260–4272 (2010).
42. E. D. Palik, *Handbook of Optical Constants of Solids* (Elsevier, 2012), Vol. **1**.
43. G. Shalev, S. W. Schmitt, H. Embrechts, G. Brönstrup, and S. Christiansen, "Enhanced photovoltaics inspired by the fovea centralis," Sci. Rep. **5**, 8570 (2015).
44. X. Guo, D. Wang, B. Liu, S. Li, and X. Sheng, "Enhanced light absorption in thin film silicon solar cells with Fourier-series based periodic nanostructures," Opt. Express **24**, A408–A413 (2016).
45. J. Hou, W. Hong, X. Li, C. Yang, and S. Chen, "Biomimetic spiral grating for stable and highly efficient absorption in crystalline silicon thin-film solar cells," Opt. Express **25**, A922–A931 (2017).
46. S. Das, M. J. Hossain, S.-F. Leung, A. Lenox, Y. Jung, K. Davis, J.-H. He, and T. Roy, "A leaf-inspired photon management scheme using optically tuned bilayer nanoparticles for ultra-thin and highly efficient photovoltaic devices," Nano Energy **58**, 47–56 (2019).
47. Y. Da and Y. Xuan, "Role of surface recombination in affecting the efficiency of nanostructured thin-film solar cells," Opt. Express **21**, A1065–A1077 (2013).
48. M. Smeets, V. Smirnov, K. Bittkau, M. Meier, R. Carius, U. Rau, and U. W. Paetzold, "Angular dependence of light trapping in nanophotonic thin-film solar cells," Opt. Express **23**, A1575–A1588 (2015).
49. J. Zhu, C.-M. Hsu, Z. Yu, S. Fan, and Y. Cui, "Nanodome solar cells with efficient light management and self-cleaning," Nano Lett. **10**, 1979–1984 (2010).
50. A. Y. Meshalkin, V. V. Podlipnov, A. V. Ustinov, and E. A. Achimova, "Analysis of diffraction efficiency of phase gratings in dependence of duty cycle and depth," J. Phys. Conf. Ser. **1368**, 022047 (2019).
51. D. Madzharov, R. Dewan, and D. Knipp, "Influence of front and back grating on light trapping in microcrystalline thin-film silicon solar cells," Opt. Express **19**, A95–A107 (2011).
52. K. Li, J. Li, C. Reardon, C. S. Schuster, Y. Wang, G. J. Triggs, N. Damnik, J. Müenchenberger, X. Wang, E. R. Martins, and T. F. Krauss, "High speed e-beam writing for large area photonic nanostructures — a choice of parameters," Sci. Rep. **6**, 32945 (2016).
53. M. Esashi, A. Kojima, N. Ikegami, H. Miyaguchi, and N. Koshida, "Development of massively parallel electron beam direct write lithography using active-matrix nanocrystalline-silicon electron emitter arrays," Microsyst. Nanoeng. **1**, 15029 (2015).
54. D. Lam, "Multibeam Corporation," http://www.multibeamcorp.com/about.htm.
55. S. V. Sreenivasan, "Nanoimprint lithography steppers for volume fabrication of leading-edge semiconductor integrated circuits," Microsyst. Nanoeng. **3**, 17075 (2017).
56. R. Seki, A. Ando, T. Motokawa, M. Suenaga, N. I. Sakurai, R. Komatsu, M. Naka, R. Taniguchi, S. Taniguchi, K. Hagihara, M. Saito, H. Sakurai, R. Yoshikawa, E. Yamanaka, and S. Kanamitsu, "Template development for sub15nm nanoimprint lithography," Proc. SPIE **11178**, 111780S (2020).
57. H. H. Solak, C. Dais, and F. Clube, "Displacement Talbot lithography: a new method for high-resolution patterning of large areas," Opt. Express **19**, 10686–10691 (2011).
58. L. Wang, F. Clube, C. Dais, H. H. Solak, and J. Gobrecht, "Sub-wavelength printing in the deep ultra-violet region using displacement Talbot lithography," Microelectron. Eng. **161**, 104–108 (2016).
59. C. Dais, F. Clube, L. Wang, and H. H. Solak, "High rotational symmetry photonic structures fabricated with multiple exposure displacement Talbot lithography," Microelectron. Eng. **177**, 9–12 (2017).
60. P. Chausse, E. Le Boulbar, P.-M. Coulon, and P. A. Shields, "'Double' displacement Talbot lithography: fast, wafer-scale, direct-writing of complex periodic nanopatterns," Opt. Express **27**, 32037–32046 (2019).
61. P. Chausse and P. A. Shields, Department of Electronic and Electrical Engineering, University of Bath, Claverton Down, Bath BA2 7AY, UK (personal communication, July 2020).
62. C. C. Nshii, M. Vangeleyn, J. P. Cotter, P. F. Griffin, E. A. Hinds, C. N. Ironside, P. See, A. G. Sinclair, E. Riis, and A. S. Arnold, "A surface-patterned chip as a strong source of ultracold atoms for quantum technologies," Nat. Nanotechnol. **8**, 321–324 (2013).